Accepted Manuscript
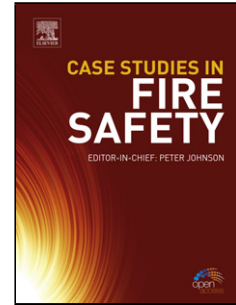
Title: The effect of Sn-VO defect clustering on Zr alloy corrosion

Author: B.D.C. Bell S.T. Murphy R.W. Grimes M.R. Wenman

Please cite this article as: B.D.C. Bell, S.T. Murphy, R.W. Grimes, M.R. Wenman, The effect of Sn-VO defect clustering on Zr alloy corrosion, <![CDATA[Corrosion Science]]> (2018), https://doi.org/10.1016/j.corsci.2018.06.020

The effect of Sn-VO defect clustering on Zr alloy corrosion

B. D. C. Bell[a], S. T. Murphy[b], R. W. Grimes[a], M. R. Wenman[a,]

[a]*Department of Materials and Centre for Nuclear Engineering, Imperial College, London, SW7 2AZ, UK*
[b]*Department of Engineering, Engineering Building, Lancaster University, Lancaster, LA1 4YW, UK*

Abstract

Density functional theory simulations were used to study Sn defect clusters in the oxide layer of Zr-alloys. Clustering was shown to play a key role in the accommodation of Sn in ZrO_2, with the $\{Sn_{Zr}:V_O\}^\times$ bound defect cluster dominant at all oxygen partial pressures below 10^{-20} atm, above which $Sn_{Zr}^\times$ is preferred. $\{Sn_{Zr}:V_O\}^\times$ is predicted to increase the tetragonal phase fraction in the oxide layer, due to the elevated oxygen vacancy concentration. As corrosion progresses, the transition to $Sn_{Zr}^\times$, and resultant destabilisation of the tetragonal phase, is proposed as a possible explanation for the early first transition observed in Sn-containing Zr-Nb alloys.

Keywords:

Density functional theory, Zirconium, Niobium, Corrosion, Hydrogen pick-up

1. Introduction

Since the very beginning of water cooled-reactors zirconium has been the fuel cladding material of choice because it offers the best combination of

neutronic, structural and corrosion properties. The first alloy regularly used in power reactors was Zircaloy-2, which contains 1.2 wt.% Sn [1, 2]. Sn was originally included as a way to mitigate the detrimental effect on corrosion associated with the N and C impurities present in the Zr-sponge, however Sn was also found to improve strength and creep resistance, and was included in the later developed Zircaloy-4 and ZIRLO alloys [1, 2, 3].

Modern Zr-sponge contain significantly less impurities, and it has been established that a reduction in Sn concentration improves the corrosion resistance of Zr-Nb alloys. For this reason it has been removed from many alloys such as M5 [4]. The role of Sn in corrosion is still poorly understood, however work performed by Wei *et al.* [5] has shown that Sn does not influence the corrosion kinetics of Zr-Nb alloys, but rather that the removal of Sn delays the onset of transition. This behaviour does seem to be limited to Zr-Nb alloys as Ortner *et al.* [6] did not observe this behaviour in a study of Zircaloy-4 and it is noted that Zr-Nb-Sn alloys seem to behave quite differently to the Zircaloy series of alloys. Further, X-ray diffraction (XRD) measurements have shown that the tetragonal ZrO_2 phase fraction increases with increasing Sn content in Nb containing alloys [5]. Garner *et al.* suggested that Sn incorporated into the oxide may therefore be one of the stabilising features of this oxide phase; other contributions are from the compressive stress, generated on transformation of metal to oxide, and the possibly very small (nano-scale) size of some tetragonal grains [7]. Recent density functional theory (DFT) studies of the role of Sn in changing the defect concentrations showed that Sn can be present in either the 2+ or 4+ charge states and that there was a critical oxygen partial pressure at which point Sn^{2+}, present at low oxygen

2

29 partial pressures, would switch to Sn^{4+} in the oxide layer [8]. Hulme *et al.*
30 used X-ray absorption near edge spectroscopy (XANES) to prove that Sn^{2+}
31 did indeed exist in the oxide layer but were not able to determine any depth
32 profile for the $2+/4+$ charge states for Sn [9]. It was postulated in both
33 papers that Sn^{2+} may have created charged oxygen vacancies to charge ba-
34 lance the Sn^{2+} cations and the presence of these oxygen vacancies in turn
35 stabilised the tetragonal phase. As the oxide layer thickens and the oxygen
36 partial pressure increases (i.e. at a position in the oxide that is further from
37 the metal-oxide interface) it was postulated that Sn^{2+} changes to Sn^{4+} on
38 reaching a critical value and the vacancies were no longer needed for charge
39 balance. This change in oxidation state of the Sn cations, and the associated
40 drop in the oxygen vacancy concentration, destabilised the tetragonal phase
41 and led to its transformation to the monoclinic phase and this in turn could
42 have initiated cracking in the oxide associated with the transition because of
43 the 4% volume increase from the tetragonal to monoclinic phases. The issue
44 with this initial theory is it did not explain why the corrosion rate does not
45 increase with increased oxygen vacancy concentration - something that was
46 observed by Bell *et al.* when Zr is doped with Sc^{3+} ions [10].

47   In this paper a set of defects are modelled in tetragonal ZrO_2 using the
48 same technique employed by Bell *et al.* [8, 10, 11]. These defects are bound
49 $\{Sn_{Zr}:V_O\}$ clusters of different configurations and charge states. It is shown
50 that certain combinations have a strong binding energy and are favoured
51 over the isolated Sn ion defects previously presented. The effect of non-
52 equilibrium charge in the oxide layer is also investigated in the formulation
53 of the Brouwer diagrams.

3

2. Methodology

DFT simulations were performed using the CASTEP 8.0 software [12], with ultra-soft pseudo potentials and a cut-off energy of 550 eV. The exchange-correlation functional was described by the Perdew, Burke and Ernzerhof (PBE) [13] formulation of the generalised gradient approximation (GGA). Integration of the Brillouin zone was performed using a Monkhorst-Pack sampling scheme [14] , with a minimum k-point separation of 0.045 Å^{-1}. The Pulay method [15] for density mixing was employed.

Self-consistent calculations were performed until an energy convergence of 1×10^{-8} eV between successive iterations was achieved. The convergence criteria for geometry optimisation were; a maximum difference in energy of 1×10^{-5} eV, an atomic displacement of 5×10^{-4} Å between iterations and a maximum force between ions of 1×10^{-2} eV/Å.

Non-defective 108 atom t-ZrO_2 and 96 atom m-ZrO_2 supercells were geometry optimised under constant (zero) pressure, from which all defective structures were subsequently generated and the energy minimised under constant volume. An energy correction calculated using the screened Madelung method [16] was used to account for the electrostatic self-interaction of defects created by the use of periodic conditions and a finite supercell size using dielectric values calculated by Zhao and Vanderbilt [17].

Each single and clustered defect in each overall charge state of interest was simulated in isolation in a supercell of the requisite ZrO_2 phase. Defect clusters consisting of a substitutional Sn atom, Sn_{Zr}, and an oxygen vacancy, V_O, (i.e. $\{Sn_{Zr}:V_O\}$) were prepared by removing the nearest O ion to the Sn_{Zr} defect. The overall charge on the cluster was varied from -2 to +2 so that the

4

79 Sn ion is able to assume a range of possible oxidation states. Defect formation

80 energies (E^f) were calculated for each defect simulated using the methodology

81 outlined in [8]. The calculated formation energies for each isolated defect

82 were then used to approximate the interactions between multiple defects, as

83 would be expected in a real oxide layer.

84 In any given defective cell, the sum of all defects multiplied by their charge

85 must equal zero, since there is no overall charge on the crystal. This can be

86 expressed as follows:

$$\sum_i q_i c_i - N_c \exp\left(-\frac{E_g - \mu_e}{k_B T}\right) + N_v \exp\left(-\frac{\mu_e}{k_B T}\right) = 0 \qquad (1)$$

87 where the first term is the sum of the charges of all ionic defects (q_i is the

88 ionic charge and c_i the concentration of ionic defect i), the second term is

89 the electron concentration and the third term the hole concentration in the

90 crystal. N_c and N_v are the density of states for the conduction and valence

91 bands, E_g is the band gap of the crystal, μ_e is the electron chemical potential,

92 k_B is the Boltzmann constant and T the temperature. The concentrations

93 c_i of each ionic defect i are calculated using the approach developed by Ka-

94 samatsu *et al.* [18], which uses standard Boltzmann statistics to calculate

95 concentrations but also accounts for ionic defects competing for the same

96 lattice site.

97 Tetragonal ZrO_2 is a wide band gap insulator, and as such the concentra-

98 tions of electrons and holes are expected to be sufficiently low that Boltzmann

99 statistics are appropriate. Self-trapping of electrons causes a reduction in the

100 formation energy of electrons in the conduction band, when compared to the

101 value calculated by $E_g - \mu_e$, however due to the wide band gap the difference

5

102 in energy is minimal and so this is an acceptable approximation [19].

103 Using the relationship in Equation 1, the electron chemical potential re-
104 quired to ensure charge neutrality for a given set of chemical potentials and
105 oxygen partial pressure, and thus the concentration of all defects ([D]), can
106 be calculated. The chemical potentials of the reactive species were obtained
107 from formation energies of the relevant oxides following established met-
108 hods [8, 19, 20, 21, 22]. The predicted defect concentrations as a function of
109 oxygen partial pressure were then plotted for each oxide to produce Brouwer
110 diagrams. As oxygen partial pressure in the oxide layer decreases with dis-
111 tance from the oxide/water interface, a Brouwer diagram can provide insight
112 into the defect concentrations through the thickness of the oxide. For all
113 diagrams, the DFT predicted band gaps of 3.40 eV for the monoclinic phase
114 and 3.95 eV for the tetragonal phase were used.

115 The approach used in this work follows the methodology outlined in pre-
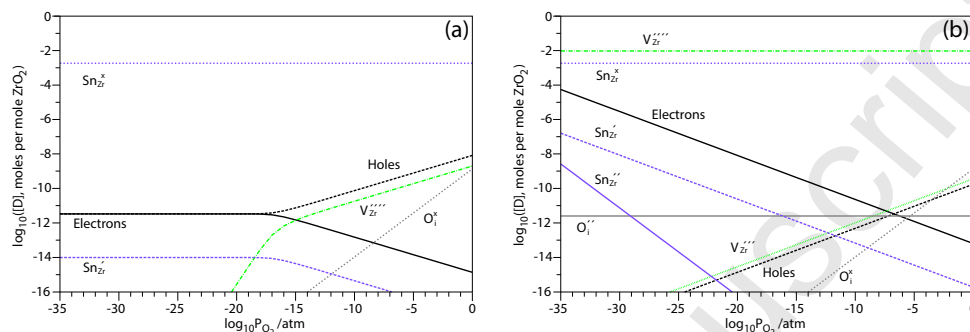116 vious work by Bell *et al.* [8, 10, 11].

6

3. Results and Discussion

Figure 1: Brouwer diagrams showing the predicted defect concentrations (plotted as the log of the concentration, in units of moles per mole of ZrO_2) in monoclinic ZrO_2 at 635 K doped with Sn at a concentration of 1×10^{-3} moles per mole of ZrO_2. The behaviour of the Sn dopant under equilibrium conditions is shown in (a). In (b) a space charge of 0.2 (moles of e⁻ per mole of ZrO_2) has been applied in order to investigate the behaviour under non-equilibrium charge conditions.

Figure 1 shows the predicted defect behaviour for monoclinic ZrO_2 doped with Sn at a concentration of 1×10^{-3} moles per mole ZrO_2. This Sn concentration, while lower than what would generally be expected for the oxide layer, was chosen to be sure that the solubility limit in the oxide phase was not exceeded. Across all oxygen partial pressures and despite the application of a high concentration of non-equilibrium charge to the system (see Figure 1b), $Sn_{Zr}^{\times}$ is predicted to be the dominant defect type. This suggests that regardless of the local conditions, Sn in monoclinic ZrO_2 should only be observed in the 4+ oxidation state.
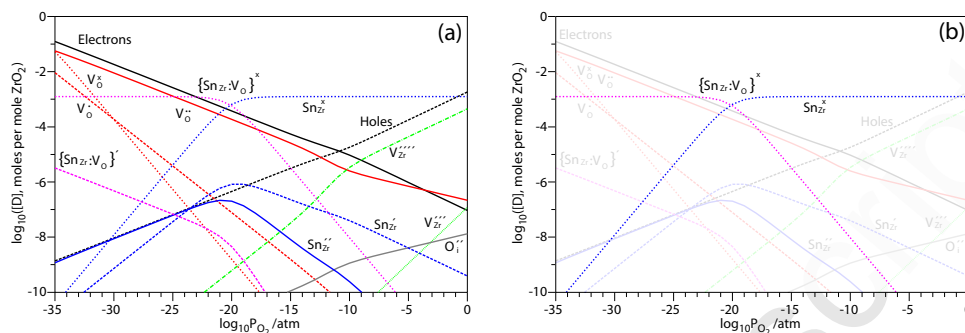
7

Figure 2: Brouwer diagrams showing the predicted defect concentrations in tetragonal ZrO_2 at 1500 K, doped with Sn at a concentration of 1×10^{-3} moles per mole of ZrO_2. $\{Sn_{Zr}:V_O\}$ clusters were simulated, and included in the diagrams as an alternative Sn defect type, with the overall Sn concentration remaining fixed. Both diagrams display the same data, however due to the complexity of the diagrams, the intrinsic and non-dominant Sn defects are partially obscured in (b) to allow the clear observation of the important Sn behaviour.

127   Previous work, investigating the behaviour of Sn in tetragonal ZrO_2, sug-
128 gested that Sn can exist in both 2+ and 4+ oxidation states in the tetragonal
129 phase and that the influence of oxygen vacancies could be significant [8]. Fi-
130 gure 2 suggests that while $Sn_{Zr}^{\times}$ remains the dominant Sn defect at high oxy-
131 gen partial pressures, below 10^{-20} atm the $\{Sn_{Zr}:V_O\}^{\times}$ bound defect cluster is
132 favoured (note: other clusters such as $\{Sn_{Zr}:V_O\}'$ that incorporate Sn^{3+} were
133 considered, but are predicted to be of negligible concentration). The binding
134 energy of $\{Sn_{Zr}:V_O\}^{\times}$ was calculated to be 1.68 eV, indicative of a strong
135 energetic preference to form a cluster. Sn_{Zr}'' has a calculated defect volume
136 of 44.22 $Å^3$, this is very large and causes a calculated stress of 6.04 GPa on
137 the 108 atom simulation supercell. Conversely $\{Sn_{Zr}:V_O\}^{\times}$ has a calculated
138 defect volume of 5.43 $Å^3$, only slightly larger than that of $Sn_{Zr}^{\times}$ (2.02 $Å^3$), sug-

8

ACCEPTED MANUSCRIPT

139 gesting that the cluster may form in preference to isolated defects in order

140 to reduce lattice stress.

141 Corrosion of Zr metal is known to occur close to the metal/oxide inter-

142 face (i.e. oxygen diffuses through the oxide layer to the metal, rather than Zr

143 ions diffusing outwards towards the environment), so the Zr-metal is oxidised

144 under a low oxygen partial pressure; conditions similar to those on the left

145 hand side of the diagrams in Figure 2. Thus, as oxidation occurs the Sn ions

146 have a strong preference to oxidise to the 2+ state and bind with an oxygen

147 vacancy to form a $\{Sn_{Zr}:V_O\}^\times$ cluster. As corrosion progresses, the metal

148 oxide interface moves deeper into the Zr-metal and the oxygen partial pres-

149 sure in the previously formed ZrO_2 gradually increases. In an intrinsic oxide

150 layer, this would lead to a gradual reduction in the oxygen vacancy concen-

151 tration, however as shown in Figure 2 the $\{Sn_{Zr}:V_O\}^\times$ clusters remain at a

152 relatively constant concentration at oxygen partial pressures below 10^{-23} atm.

153 The presence of the Sn ions, therefore, results in an increased oxygen vacancy

154 concentration in the tetragonal phase of the oxide layer. Since oxygen va-

155 cancies are known to stabilise the tetragonal phase of ZrO_2, the presence of

156 Sn in the oxide layer results in an increased tetragonal phase fraction. This

157 result agrees well with XRD work [5], which reported that as the Sn content

158 of ZIRLO was reduced, the measured tetragonal phase fraction also reduced.

159 As discussed in the introduction, previous work suggested that an increa-

160 sed oxygen vacancy concentration may lead to an increased tetragonal phase

161 fraction in Zr-based alloys. However, what has not previously been discussed

162 is why the increased oxygen vacancy concentration in Sn-containg Zr alloys

163 does not lead to an elevated corrosion rate, as is observed in other similar sy-

9

Page 9 of 15

164 stems (for example, Sc^{3+} dramatically increases both the the oxygen vacancy

165 concentration and the corrosion rate in Zr-based alloys [10]). As shown in

166 Figure 3, the pre-transition corrosion rate does not appear to be influenced

167 at all by the Sn content of the alloy, rather the increased long-term corrosion

168 behaviour observed in Sn-containing alloys appears to be due to an earlier
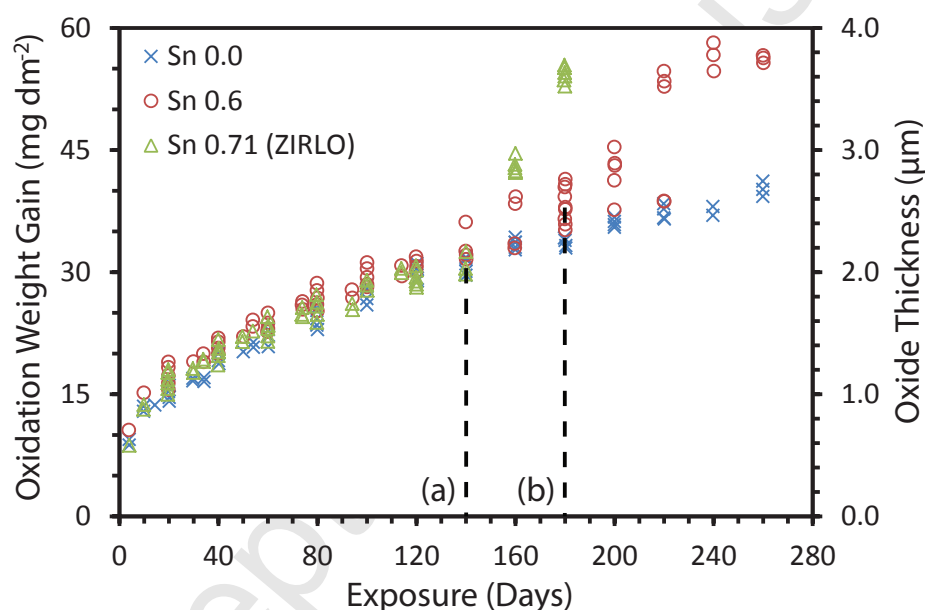
169 transition occurring in high Sn alloys.

Figure 3: Oxide weight gain results showing no change in pre-transition corrosion rate but an earlier first transition in Sn-containing Zr alloys containing: 0.71 (ZIRLO), 0.51 and 0.01 at.% Sn. The dashed lines have been added to show the approximate point of early transition for (a) 0.71 at.% Sn (ZIRLO) after 140 days and (b) 0.51 at.% Sn after 180 days of autoclave corrosion. Corrosion was performed in an autoclave at 360 °C in simulated primary water at a saturation pressure of ˜18 MPa. (Data replotted from [5]).

170 This study suggests that the additional oxygen vacancies resulting from

171 the inclusion of Sn in the oxide layer exist only in bound $\{Sn_{Zr}{:}V_O\}^{\times}$ clus-

10

172 ters and thus while the vacancy concentration, (and hence tetragonal phase
173 fraction) is increased, the additional vacancies are assumed to have limited
174 mobility and so do not cause a measurable increase in the corrosion rate of
175 the alloy. As corrosion progresses, the oxygen partial pressure experienced
176 by the Sn ions in the oxide layer increases as the metal/oxide interface moves
177 deeper into the Zr-alloy. Once the oxygen partial pressure reaches 10^{-20} atm,
178 $Sn_{Zr}^{\times}$ becomes more energetically favourable than the $\{Sn_{Zr}:V_O\}^{\times}$ clusters.
179 $Sn_{Zr}^{\times}$ does not require the presence of an oxygen vacancy for charge neutra-
180 lity, and so the oxygen vacancy concentration in the oxide layer is reduced.
181 Thus, the change in preferred Sn oxidation state results in tetragonal phase
182 stabilising oxygen vacancies being removed from the lattice. This is likely to
183 trigger a transformation of the tetragonal phase into the monoclinic phase.
184 The tetragonal to monoclinic phase transformation is associated with a 4%
185 increase in unit cell volume, causing buckling and cracking of the layer and
186 potentially triggering the earlier first transition observed in Sn containing
187 Zr-Nb alloys. As this phase transformation is driven by the presence of Sn
188 ions in the oxide lattice, it is expected that the effect would be increasingly
189 effective at triggering an early first transition with increasing Sn content.
190 This agrees well with the results reproduced in Figure 3, which show that
191 alloys containing a higher Sn content undergo increasingly early first transi-
192 tion; 0.51 at.% Sn after approximately 180 days and 0.71 at.% Sn after 140
193 days.

11

4. Conclusions

1. Sn^{4+} is the dominant defect type across all oxygen partial pressures in monoclinic ZrO_2.

2. Sn^{2+} is dominant at low oxygen partial pressures in tetragonal ZrO_2, transitioning to Sn^{4+} above 10^{-20} atm.

3. Sn^{2+} forms bound $\{Sn_{Zr}:V_O\}^{\times}$ clusters with an oxygen vacancy, increasing the oxygen vacancy concentration and thus stabilising the tetragonal phase, but bound clusters prevent the increased V_O concentration from changing the corrosion rate.

4. As corrosion progresses and $\{Sn_{Zr}:V_O\}^{\times}$ transitions to Sn^{4+}, the additional oxygen vacancies are no longer required in the system and the tetragonal phase stabilisation is lost.

5. The destabilised tetragonal phase transforms to monoclinic with an associated increase in volume of around 4%, possibly triggering the early oxide layer transition observed in Sn-containing Zr alloys.

6. The early transition triggered by the change in Sn oxidation state is expected to be more apparent with increased Sn-content.

5. Acknowledgements

[1] K. Balaramamoorthy. Current Trends in the Use of Zirconium Alloys.

12

217 Technical report, Atomic Fuels Division, Bhabha Atomic Research Cen-
218 tre, Bombay, 1968.

219 [2] ATI. Reactor Grade Zirconium Alloys for Nuclear Waste Disposal.
220 Technical report, Allegheny Technologies Incorporated, 2003.

221 [3] K. Natesan and W.K. Soppet. Hydrogen effects on air oxidation of zirlo
222 alloy. Technical report, 2004.

223 [4] J. P. Mardon, D. Charquet, and J. Senevat. Influence of composition and
224 fabrication process on out-of-pile and in-pile properties of M5 alloy. In
225 *Zirconium in the Nuclear Industry: Twelfth International Symposium,*
226 *ASTM STP 1354*, pages 505–524, 2000.

227 [5] J. Wei, P. Frankel, E. Polatidis, M. Blat, A. Ambard, R. J. Com-
228 stock, L. Hallstadius, D. Hudson, G. D. W. Smith, C. R. M. Grovenor,
229 M. Klaus, R. A. Cottis, S. Lyon, and M. Preuss. The effect of Sn on
230 autoclave corrosion performance and corrosion mechanisms in Zr-Sn-Nb
231 alloys. *Acta Materialia*, 61(11):4200–4214, 2013.

232 [6] S. Ortner, H. Swan, A. Laferrere, C. English, J. Hyde, and P. Styman.
233 Study Of Zircaloy Corrosion To Develop Mechanistic Understanding. In
234 *Contribution of Materials Investigations and Operating Experience to*
235 *LWRs Safety, Performance and Reliability*, 2014.

236 [7] A. Garner, J. Hu, A. Harte, P. Frankel, C. R. M. Grovenor, S. Lozano-
237 Perez, and M. Preuss. The effect of Sn concentration on oxide tex-
238 ture and microstructure formation in zirconium alloys. *Acta Materialia*,
239 99:259–272, 2015.

13

[8] B. D. C. Bell, S. T. Murphy, P. A. Burr, R. W. Grimes, and M. R. Wenman. Accommodation of tin in tetragonal ZrO2. *Journal of Applied Physics*, 117:084901, 2015.

[9] H. Hulme, F. Baxter, R. P. Babu, M. A. Denecke, M. Gass, A. Steuwer, K. Noren, S. Carlson, and M. Preuss. An X-ray absorption near-edge structure (XANES) study of the Sn L3 edge in zirconium alloy oxide films formed during autoclave corrosion. *Corrosion Science*, 105:202–208, 2015.

[10] B. D. C. Bell, S. T. Murphy, P. A. Burr, R. J. Comstock, J. M. Partezana, R. W. Grimes, and M. R. Wenman. The influence of alloying elements on the corrosion of Zr alloys. *Corrosion Science*, 105:36–43, 2016.

[11] B. D. C. Bell, S. T. Murphy, R. W. Grimes, and M. R. Wenman. The effect of Nb on the corrosion and hydrogen pick-up of Zr alloys. *Acta Materialia*, 2017.

[12] S. J. Clark and M. D. Segall. First principles methods using CASTEP. *Zeitschrift fur Kristallographie*, 220:567–570, 2005.

[13] J. Perdew, K. Burke, and M. Ernzerhof. Generalized Gradient Approximation Made Simple. *Physical Review Letters*, 77(18):3865–3868, 1996.

[14] H. J. Monkhorst and J. D. Pack. Special points for Brillouin-zone integrations. *Physical Review B*, 13(12):5188–5192, 1976.

[15] P. Pulay. Convergence Acceleration of Iterative Sequences. The Case of SCF Iteration. *Chemical Physical Letters*, 73(2):393–398, 1980.

14

[16] S. T. Murphy and N. D. M. Hine. Anisotropic charge screening and supercell size convergence of defect formation energies. *Physical Review B - Condensed Matter and Materials Physics*, 87(9):1–6, 2013.

[17] X. Zhao and D. Vanderbilt. First-principles study of structural, vibrational, and lattice dielectric properties of hafnium oxide. *Physical Review B*, 65(23):075105–1–10, 2002.

[18] S. Kasamatsu, T. Tada, and S. Watanabe. Parallel-sheets model analysis of space charge layer formation at metal/ionic conductor interfaces. *Solid State Ionics*, 226(1):62–70, 2012.

[19] S. T. Murphy, M. W. D. Cooper, and R. W. Grimes. Point defects and non-stoichiometry in thoria. *Solid State Ionics*, 267:80–87, 2014.

[20] M. W. Finnis, A. Y. Lozovoi, and A. Alavi. The Oxidation of NiAl: What Can We Learn from Ab Initio Calculations? *Annual Review of Materials Research*, 35(1):167–207, 2005.

[21] H. A. Tahini, A. Chroneos, S. T. Murphy, U. Schwingenschloogl, and R. W. Grimes. Vacancies and defect levels in III-V semiconductors. *Journal of Applied Physics*, 114(6):063517, 2013.

[22] S. T. Murphy and N. D. M. Hine. Point defects and non-stoichiometry in Li 2 TiO 3. *Chemistry of Materials*, 26(4):1629–1638, 2014.

15